Gap Junction Structures. IV. Asymmetric Features Revealed by Low-irradiation Microscopy

T. S. BAKER, D. L. D. CASPAR, C. J. HOLLINGSHEAD, and D. A. GOODENOUGH
Rosenstiel Basic Medical Sciences Research Center, Brandeis University, Waltham, Massachusetts 02254; and Department of Anatomy, Harvard Medical School, Boston, Massachusetts 02115

ABSTRACT Micrographs of mouse liver gap junctions, isolated with detergents, and negatively stained with uranyl acetate, have been recorded by low-irradiation methods. Our Fourier-averaged micrographs of the hexagonal junction lattice show skewed, hexameric connexons with less stain at the threefold axis than at the six indentations between the lobes of the connexon image. These substructural features, not clearly observed previously, are acutely sensitive to irradiation. After an electron dose less than that normally used in microscopy, the image is converted to the familiar doughnut shape, with a darkly stained center and a smooth hexagonal outline, oriented with mirror symmetry in the lattice. Differences in appearance among 25 reconstructed images from our low-irradiation micrographs illustrate variation in staining of the connexon channel and the space between connexons. Consistently observed stain concentration at six symmetrically related sites ~34 Å from the connexon center, 8° to the right or left of the (1, 1) lattice vector may reveal an intrinsic asymmetric feature of the junction structure. The unexpected skewing of the six-lobed connexon image suggests that the pair of hexagonal membrane arrays that form the junction may not be structurally identical. Because the projected image of the connexon pair itself appears mirror symmetric, each pair may consist of two identical connexon hexamers related by local (noncrystallographic) twofold axes in the junctional plane at the middle of the gap. All connexons may be chemically identical, but their packing in the hexagonal arrays on the two sides of the junction appears to be nonequivalent.

Gap junctions in liver (13, 28) and many other tissues (5, 10) are built of connexon units (6) hexagonally arrayed with crystallike regularity in the pair of connected cell membranes. Makowski et al. (21) proposed a model for the junction structure based on data from x-ray diffraction, electron microscopy and chemical analysis in which the connexon units were pictured as symmetric hexamers of identical connexin molecules that are equivalently paired across the gap with dihedral symmetry in the two-sided hexagonal plane group (p622; see reference 16). This model predicts that, as normally viewed in electron micrographs of untilted, negatively stained specimens, the junction lattice should appear mirror-symmetric in projection (with p6m plane group symmetry).

Conventional high-irradiation micrographs of negatively stained specimens show doughnut-shaped connexons that appear nearly circularly symmetric in the Fourier-averaged images, and, therefore, the hexagonal lattice array, appear to have mirror symmetry (6). Higher resolution, hexagonally averaged reconstructions calculated by Zampighi and Unwin (33) from minimal irradiation micrographs of two forms of gap junctions, negatively stained with uranyl acetate, showed hexagonal shaped connexons arrayed with approximate mirror symmetry in the projected lattice images. However, the hexagonally shaped connexon images occured in two different orientations: edge-to-edge in one lattice form and vertex-to-vertex in the other. Images of gap junction lattices without mirror symmetry were obtained by Henderson et al. (14) in low-irradiation micrographs of phosphotungstate stained specimens. Their optically filtered images showed connexon pairs in projection with pronounced hexagonal substructure oriented with the hexagonal vertices inclined at an angle of ~12° to the principal lattice vectors. This asymmetry, if intrinsic to the structure, implies possible differences in conformation or packing of the connexons in the two membrane lattices that form the junction.

Regulation of intercellular junctional communication presumably involves opening and closing the channel extending along the axes of the pairs of connexons (19). Considerable variability in the accessibility of the channel to negative stain is observed in micrographs of isolated junctions (6). Some specimens show practically no stain in the center of the con-

THE JOURNAL OF CELL BIOLOGY · VOLUME 96 JANUARY 1983 204-216

nexons (14). Prolonged exposure of isolated junctions to deionized water alters the appearance of the stain-filled channel (32, 33). X-ray diffraction data from isolated junctions in sucrose solutions show that sucrose fills the extracellular gap but fails to enter the axial channel (21); this observation indicates that the channel in the isolated junctions is closed to small molecules at both cytoplasmic surfaces. Because cellular damage leads to uncoupling of junctional communication (18), the isolated junctions should be in the high resistance state. This occluded state of the channel appears to be maintained in the hydrated specimens examined with x-rays, but the stresses on specimens examined in the electron microscope may rupture the closed orifice.

Conditions which best preserve specimens for electron microscopy yield noisy images with little contrast (31). Extracting information from these micrographs requires the use of image-averaging methods (4). Our low-irradiation micrographs of gap junction specimens have been analyzed by Fourier methods for correlation with the results of our x-ray diffraction studies (6, 20, 21). The Fourier-averaged images provide new information about the symmetry of the structure, about the sensitivity of the stain distribution to electron irradiation, and about the variability in the staining.

MATERIALS AND METHODS

Purified Gap Junction Specimens: Mouse liver gap junctions were isolated from 100 animals using the protocol published previously (8). The protocol was scaled up to handle 100 animals using the Beckman Ti-15 zonal rotor (Beckman Instruments, Inc., Palo Alto, CA) according to Goodenough (12). The preparation involves initial isolation of a plasma membrane fraction by homogenization of freshly dissected livers in 1 mM $NaHCO_3$ and 1 mM EGTA, pH 8.0, followed by zonal centrifugation with a sucrose step gradient. Nonjunctional membranes are solubilized by treatment with 0.5% Sarkosyl NL-97 and the junctions are enriched by treatment with 0.1% Brij 58. Subsequent fractionation with deoxycholate, used previously (8), was omitted in this preparation and no exogenous enzymes were used.

Electron Microscopy: Specimens were prepared for electron microscopy by applying a droplet of sample (0.1–0.5 mg/ml) to a carbon-coated grid, washing with distilled water, and staining with an unbuffered 1% aqueous solution of uranyl acetate at room temperature. Grids were examined in a Philips EM301 electron microscope, usually at × 40,000–45,000 and 80 kV, using conventional or low-irradiation procedures. Conventional images were those obtained when no precautions were taken to limit the exposure of the sample to the electron beam during searching, focusing, and astigmatism corrections. The techniques used to record low-exposure images and calibrate the microscope exposure meter (to determine dose rates) are described by Baker and Amos (2). The minimal-irradiation method kept the specimen essentially unexposed and undamaged before the recording of the micrograph (a total dose of <0.1 $e^-/Å^2$ is normally delivered during the search for a suitable specimen).

Positively stained specimens were prepared by incubating a sample (~0.01 mg/ml) for 1 h with 10^{-4} M uranyl acetate, centrifuging, resuspending the pellet in water, and then adsorbing the junctions to the carbon-coated grid.

Image Processing: Over 150 gap junction images were surveyed by optical diffraction (29) to assess the electron microscope imaging conditions (defocus, astigmatism, drift, etc.) and to identify the best preserved specimen areas for further digital processing. The number and sharpness of spots in the optical diffraction pattern provided a reliable measure of the resolution and preservation of crystalline order in the specimens.

Images of 18 high-irradiation and 26 low-irradiation specimens were digitized on a 512 × 512 pixel array using an Optronics P1000 Photoscan rotating-drum microdensitometer (Optronics International, Chelmsford, MA) with a 25-μm scan raster and aperture. The digital images were displayed on a 256 grey level TV graphics screen (Grinnell Systems Corp., Santa Clara, CA). Suitable areas (usually 400 × 400 pixels containing about 900 connexon images) were boxed using the TV screen cursors and the floated density array (average density at the box perimeter subtracted from all values within the box) were Fourier-transformed on a PDP 11/40 minicomputer (Digital Equipment Corp., Maynard, MA).

Transform amplitudes were displayed on the TV screen and best coordinates of the diffraction maxima for an ideal reciprocal lattice with p1 plane group symmetry (see reference 15) were determined by a least-squares fit of the peak positions for 10–15 sharp, high intensity, spots. A single amplitude (integrated, background-corrected value) and phase measurement (at the peak position) for the structure factors at each of the ideal reciprocal lattice points out to the fifth order were calculated from the computed transform using a method described by Baker and Amos (2). This Fourier-averaging of the ~900 connexon images generates 45 unique structure factor measurements out to a resolution limit of 14.5 Å. The 45 data points for each p1 symmetry averaged transform were then averaged with p6 plane group symmetry after locating the best sixfold phase origin. Hexagonally symmetric lattice images were computed by Fourier transforming the 15 p6 averaged structure factors and the images were displayed and photographed directly from the TV screen. The regularity of the hexagonal symmetry in the original image was assessed by evaluating the crystallographic R-factor comparing the structure factor amplitudes for the p1 with the p6 averaged transforms. The R-factor, comparing two transforms, i with j, is defined as $R_F = \Sigma\|F_i| - |F_j\|/\Sigma|F_j|$, where the sum is taken over the measured set of structure factors F_{hk} with indices h, k.

The sets of structure factors for different images were put on a common scale to permit direct comparison of relative density fluctuations in the reconstructed images, and to permit unbiased averaging together of the data sets. After first setting the average density of each image equal to zero (i.e., $|F_{00}| = 0$), transforms were multiplied by linear factors to put them all on the same scale. Each transform was scaled to one chosen as reference by determining the factor that equated $\Sigma|F_{hk}|$ for the common structure factors. Tests of an alternate procedure, in which all images were scaled to have the same density in the region of maximum stain exclusion, resulted in linear scale factors nearly identical to those obtained using the $\Sigma|F|$ method. Averages of different reconstructed images were calculated by summing the corresponding structure factors, F_{hk}, from each of the data sets scaled on $\Sigma|F_{hk}|$.

The magnitude of $|F_{00}|$ for each image depends on the amount of stain in the specimen and on the exposure time for recording the micrograph. Most gap junction specimens appear to be embedded in similar amounts of stain. Differences in average image density that might result from different exposure times and stain density were minimized by the scaling procedure.

All steps in the image analysis were tested using model data to assure that the new structural features revealed in the reconstructions were not a result of artifacts in the data processing.

Conventions: The hand of structural features recorded in the micrographs was preserved by adopting a set of self-consistent conventions to maintain the same direction of view for each step in imaging, digitization, display, and photographic reproduction. The relative image intensity of the scaled reconstructions in Figs. 3 and 5 were carefully maintained by photographing the TV screen, developing the film and printing under identical conditions. Since mirror symmetry was not imposed on the hexagonally averaged lattice transforms, structure factors with indices h,k and k,h can be different. The hexagonal lattice indices are assigned as illustrated by Zampighi and Unwin (33) for their gap junction diffraction patterns. The hand of the image can be defined by the amplitude ratio of the structure factors $F_{1,2}$ and $F_{2,1}$ (see Results). With the conventions adopted $|F_{1,2}| > |F_{2,1}|$ corresponds to a left-handed image. To invert the hand of an image, the structure factors with indices h,k and k,h are interchanged. Averages were computed of all left handed images and of all right handed images; the two averages were combined by inverting one to have the same hand as the other.

RESULTS

Junction Morphology

The isolation procedure used in this study leads to extensive vesiculation of the paired membrane lattices (8). Curvature is evident in sectioned, embedded specimens. When the junctions are negatively stained, they lie flat on the grid. A majority of the negatively stained junctions appear to be broken vesicles, or flattened cup shapes. When a vesicle collapses, the two paired lattices from the two sides superimpose. Nevertheless, many separate junction lattices are observed which may arise from broken vesicles. Most of the images that were selected for processing were of non-overlapped junction patches.

Micrographs of separate junction patches recorded either at low or high irradiation often show only a single hexagonal lattice domain (Fig. 1). Some well-ordered single lattice domains are as large as 1 μm^2. The lattice in folded over junctions from flattened vesicles often appears continuous on the two sides. In many cases, however, two or more hexagonal lattice domains with different orientations can be distinguished in a single junction. Most of the junction images selected for proc-

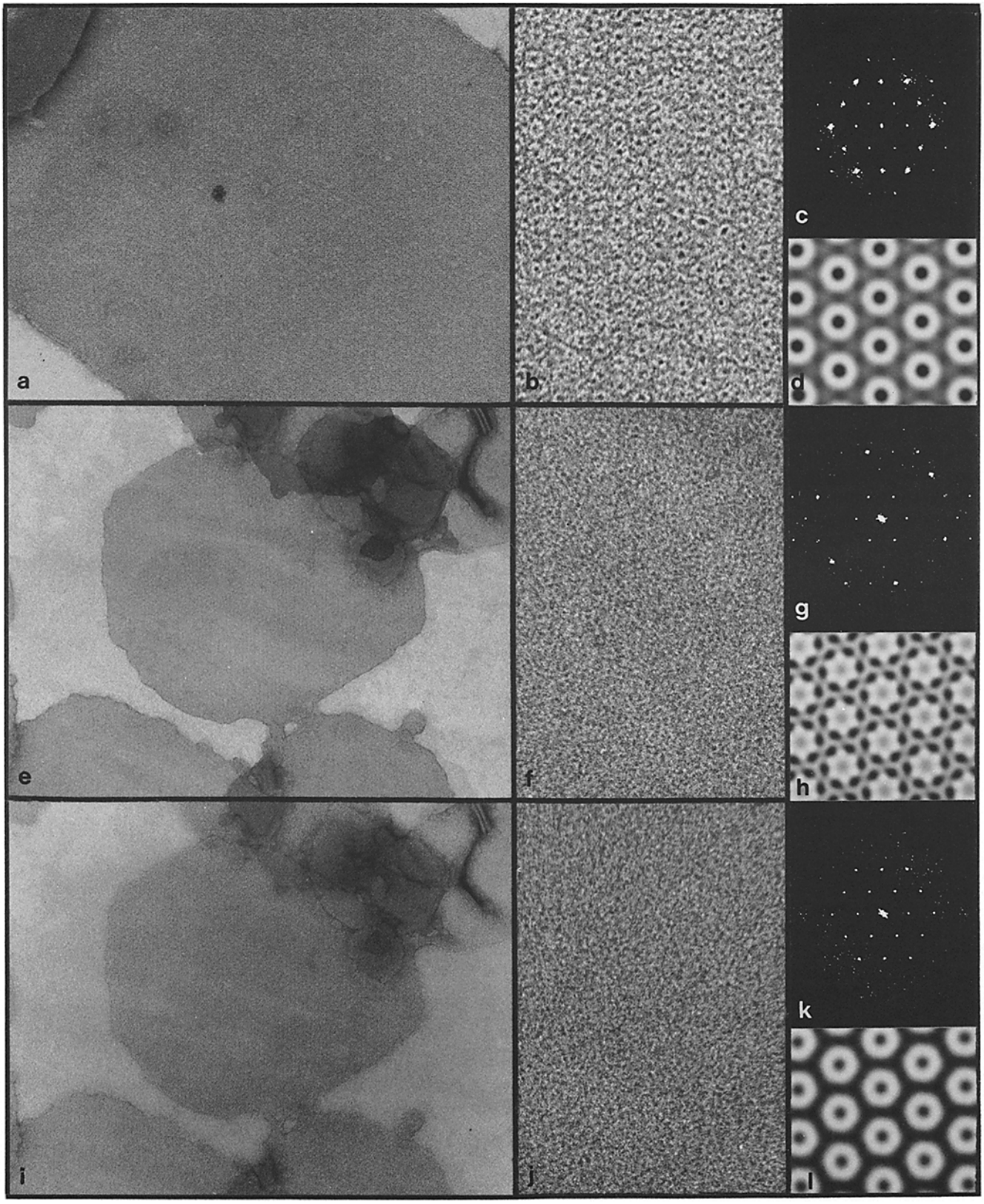

FIGURE 1 Comparison of high and low-irradiation gap junction images. Three gap junction micrographs, one recorded (*a*) conventionally with high-irradiation (total dose ~200–500 $e^-/Å^2$) and two from the same specimen, first recorded (*e*) with low irradiation (~20$e^-/Å^2$) and then recorded again with a weak beam (*i*) after receiving a total dose of ~100–200 $e^-/Å^2$. (*a*, *e*, and *i*) × 100,000. (*b*, *f*, and *j*) Enlarged views of well-ordered domains in center: (*b*, *f*, and *j*) × 500,000. Diffraction patterns (*c*, *g*, *k*) are computed from regions about four times larger than the lattice domains shown at × 500,000; *g* and *k* are transforms of identical areas from the same junction shown in *f* and *j*. Fourier-averaged images (*d*, *h*, and *l*) were reconstructed with p6 lattice symmetry from the computed diffraction patterns (*c*, *g*, and *k*) and are displayed at an equivalent magnification of × 1,000,000.

essing consisted of single lattice domains, but in some cases two differently oriented lattices were analyzed from one junction patch.

Radiation Sensitivity and Image Appearance

Fourier-averaged, low-irradiation images of our uranyl acetate-stained gap junction specimens are significantly different from conventional, high-exposure images (Fig. 1). The new structural features are radiation sensitive since further irradiation leads to images quite similar to the conventional ones (compare Fig. 1 *d* and *l*). The dominant connexon image, readily visible in unprocessed conventional micrographs (Fig. 1 *a* and *b*) is not easily recognized in low-exposure micrographs (e.g., Fig. 1 *e* and *f*) or subsequently following further irradiation (Fig. 1 *i* and *j*) of specimens which received an initial minimal dose. The high contrast of the conventional image may be an artifact of the initial exposure to an intense electron beam (>25 $e^-/Å^2/s$), whereas exposure of the specimens to a diffuse, weaker beam (2–5 $e^-/Å^2/s$) appears to fix[1] the specimen in a low-contrast state, that is, nevertheless, still sensitive to radiation damage. Because these images obtained with a weak electron beam (Fig. 1 *f* and *j*) have low contrast and therefore a low signal-to-noise ratio, image averaging is essential to reveal the intrinsic features (Fig. 1 *h* and *l*) of the connexon images in the periodic arrays. Comparison of reconstructed images of minimally irradiated specimens (e.g., Fig. 1 *h*) with reconstructions of high-irradiation images (e.g., Figs. 1 *d* and *l*) clearly illustrates the substantial rearrangement in the stain distribution induced by the electron beam.

The connexon image obtained with minimal irradiation (Fig. 1 *h*) shows asymmetrically oriented hexagonal substructure and a weakly stained center in contrast to the doughnut-shaped high-irradiation images (Fig. 1 *d* and *l*). In the low-irradiation image (Fig. 1 *h*) less stain is seen near the threefold unit cell position than at the six indentations between the lobes of the connexon. The asymmetric orientation of the hexagonal connexon image in the lattice suggests a possible asymmetry in the structure of the two halves of the gap junction (see Discussion). The features noted in this image are characteristic of low-irradiation micrographs although there is considerable variation in the appearance of different junctions. Variability may result from specimen alterations and/or differences in the staining. From more than 100 low-irradiation junction images surveyed by optical diffraction, the 25 selected for quantitive analysis illustrate a wide range of appearances of common structural features in well-ordered gap junction lattices.

Hexagonal Lattice Symmetry

The lattice dimensions of many gap junction specimens, measured from computed diffraction patterns of both low-irradiation and conventional micrographs, are nearly perfectly hexagonal. Some specimens are obviously distorted due to surface tension effects on drying or irregularities in the grid surface; and others have lattice defects that limit the size of coherently diffracting domains. Lattice distortions were recognized by examination of the micrographs or their optical diffraction patterns. Measurements of cell dimensions on 29 specimens all recorded at × 45,000, which were judged to be

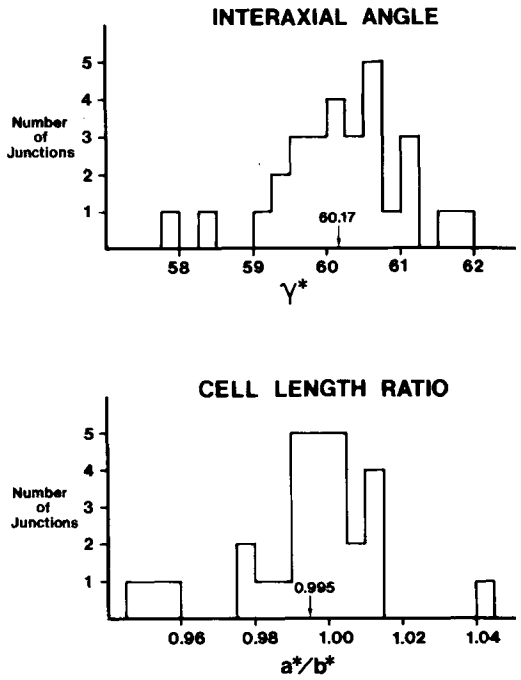

FIGURE 2 Hexagonal lattice symmetry of gap junction images. Reciprocal lattice parameters, measured from the computed diffraction patterns of 26 low- and 3 high-irradiation gap-junction images, and plotted as histograms, demonstrate excellent agreement of the experimental data with an ideal hexagonal lattice. The mean values for the interaxial diffraction cell angle, $\bar{\gamma}^* = 60.17 \pm 0.87°$, and the ratio of the reciprocal lattice cell lengths, $\bar{a}^*/\bar{b}^* = 0.995 \pm 0.020$, agree with the values (60° and 1.0) expected for a perfect hexagonal lattice. The average value of the unit cell constant is $a = 84 \pm 2$ Å.

free of obvious distortions, are summarized in Fig. 2. The value of the angle between the reciprocal lattice unit vectors is very close to 60° and the two unit vectors have nearly the same length as expected for a regular hexagonal lattice. The average lattice constant for these specimens is 84 Å with a standard deviation of ±2 Å. Small distortions in the hexagonal cell shape in some of these junctions lattices does not have a significant effect on the symmetry of the averaged connexon image.

Hexagonal shape of the unit cell does not require that its contents have hexagonal symmetry. Hexagonal symmetry in the junction images selected for processing is directly indicated by the amplitudes and phases of the hexagonally related strong spots in the computed diffraction patterns (Fig. 1 *c*, *g*, and *k*); some weak spots show departures from hexagonal regularity but the noise level is close to their measured amplitude. Initial averaging of the Fourier transform with p1 plane group symmetry generates three independent structure factors corresponding to each p6 lattice structure factor. The R-factors comparing the amplitudes of the p1 averaged data with the p6-average for 25 low-irradiation images are in the range 11–32%, and the average R-factor is 22%. That is, the mean variation in amplitude among sets of three spots that should be identical if the hexagonal symmetry were perfect is on the order of 20%. This variation is comparable to, or less than, that between the transforms of adjacent pairs of junction lattices in the same micrograph. The R-factor for the most closely correlated adjacent pair of processed lattice images is 16%, whereas some adjacent pairs have R-factors of ~30%. Thus, the departures from perfect hexagonal symmetry measured in individual junc-

[1] Others have shown that a weak beam somehow stabilizes specimens (1, 7, 17). Nevertheless, the stain distribution is still sensitive to the effects of further irradiation (3).

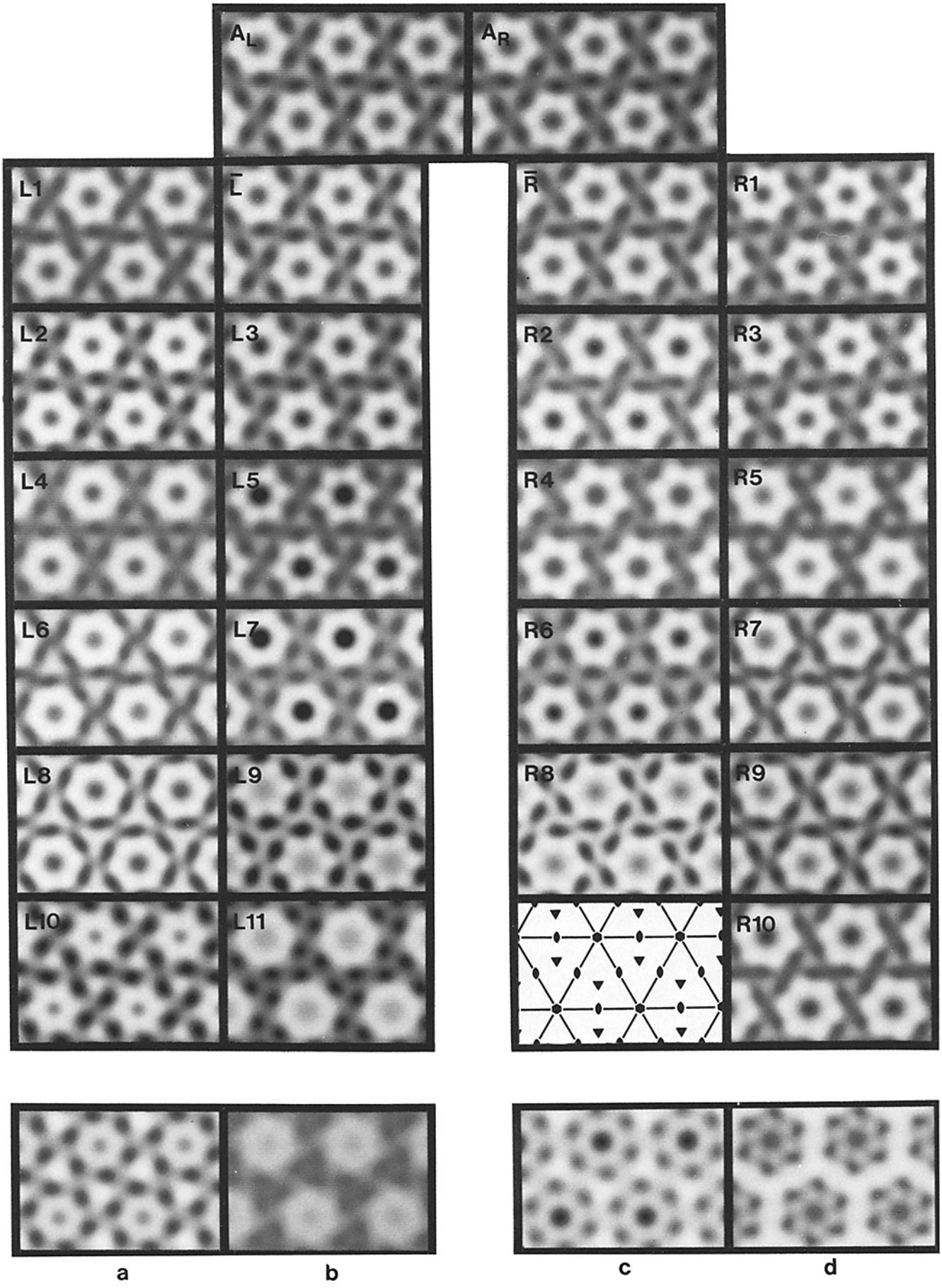

KEY TO FIGURE 3

	A_L Average of $\bar{L}$ and $\bar{R}$ (turned L)	A_R Average of $\bar{R}$ and $\bar{L}$ (turned R)	
L1 / Ia$_1$ $R_F = 0.165$	$\bar{L}$ Average of L1–L11	$\bar{R}$ Average of R1–R10	R1 / Ia$_3$ $R_F = 0.175$
L2 / Ib $R_F = 0.177$	L3 / IVa $R_F = 0.220$	R2 / IIa$_1$ $R_F = 0.206$	R3 / Ia$_4$ $R_F = 0.197$
L4 / Ia$_2$ $R_F = 0.302$	L5 / IIa$_2$ $R_F = 0.331$	R4 / IIa$_3$ $R_F = 0.326$	R5 / IIa$_4$ $R_F = 0.256$
L6 / Ic $R_F = 0.258$	L7 / VIa $R_F = 0.494$	R6 / IIb $R_F = 0.276$	R7 / Ie $R_F = 0.247$
L8 / Id $R_F = 0.416$	L9 / IIc $R_F = 0.515$	R8 / IId $R_F = 0.456$	R9 / If $R_F = 0.368$
L10 / Va$_1$ $R_F = 0.355$	L11 / IVb$_1$ $R_F = 0.549$	p6 Lattice	R10 / IIIa $R_F = 0.419$
a Va$_2$ $R_F = 0.601$ (0.752)	*b* IVb$_2$ $R_F = 0.557$ (0.722)	*c* Ig Weakly stained	*d* IIe Postively stained

FIGURE 3 Variable and consistent features in new gap junction images. This gallery of individual (L1–L11, R1–R10; *a–d*) and average (A_L, A_R, $\bar{L}$, $\bar{R}$) reconstructions of low-irradiation micrographs shows that consistent features are revealed, although there is a wide range of variation in the detailed stain distributions in the gap junction specimens. The reconstructions are grouped according to whether the connexon image is left- (L1–L11) or right-handed (R1–R10). $\bar{L}$ is the average of the eleven left-handed images, and $\bar{R}$ is the average of the ten right-handed images. A_L and A_R are averages of all 21 reconstructed images, inverted as necessary to have the same hand. In all reconstructions included in the averages, the density fluctuations are put on the same relative scale (see Materials and Methods). The lattice diagram depicts the location of symmetry elements for the p6 hexagonal plane group. *a–d* are reconstructions, not included in the averages, from very low contrast micrographs that have been rescaled for comparison with the rest. The key, above, identifies the specimens and tabulates the R-factors comparing image transforms. Specimens were derived from six different preparations designated I–VI; the lower case letters designate different micrographs from each preparation; and the numerical subscripts designate different junction lattice domains in the same micrograph. The R-factors, designated R_F, compare the transforms of individual left-handed images with their average $\bar{L}$, and similarly for right-handed images with their average $\bar{R}$. Two values of R_F are listed for images *a* and *b*: the one in parentheses is for scaling the transforms on $\Sigma|F|$ as for all the L and R images; and a smaller one after rescaling to minimize the R-factor. R-factors are not listed for images *c* and *d* since the staining of these specimens is different from the others.

tion domains are in the same range as the image variations among adjacent junctions due to differences in stain distribution and other specimen irregularities. Averaging together different p1-averaged transforms reduces the fluctuations from hexagonal symmetry, as expected. We conclude that there are no statistically significant departures from hexagonal symmetry in the well-ordered images we have analyzed.

On the expectation that the pair of hexagonal membrane lattices that form the junction are equivalently related (6), the lattice image should appear mirror-symmetric in projection with p6m plane group symmetry. Mirror-symmetry requires that structure factors with indices h,k and k,h be equal. We consistently observe absence of mirror symmetry in the diffraction patterns of our low-irradiation images. Of the spots for which $h \neq k$, the [1, 2] or the [2, 1] spot is always one of the strongest in the diffraction pattern (cf. Fig. 1 *g*); the weaker spot of this pair has an amplitude which is generally less than half that of the stronger. This large asymmetry in the diffraction pattern of the low-irradiation images contrasts with the nearly mirror symmetric patterns from high-irradiation images (compare Fig. 1 *g* with *c* and *k*).

Structure Factors

Table I compares averaged structure factors for 21 of our low-irradiation images with those for 16 of our conventional, high-irradiation images (and also the low-irradiation data of Zampighi and Unwin [33; see Discussion]). Each average was computed from the sum of the individual transforms, inverted as necessary to maintain $|F_{1,2}| > |F_{2,1}|$ (which makes all transforms left-handed according to our convention). For the 25 low-irradiation images illustrated in Fig. 3 (processed maintaining the same direction of view for all micrographs), 13 are left-handed ($|F_{1,2}| > |F_{2,1}|$) and 12 right-handed ($|F_{1,2}| < |F_{2,1}|$); there is no ambiguity in hand assignment since the difference in amplitude for the two spots is always much greater than the uncertainty in the measurement. Out of these 25 images, two left-handed and two right-handed ones were omitted from the average in Table I since they differed in significant structural detail (see below).

Asymmetry in the conventional, high-irradiation images is generally very weak, although a hand can be assigned from the small difference in amplitude of the [1, 2] and [2, 1] spots. For the 16 transforms computed from the conventional images, seven are left-handed and nine are right-handed according to our convention; however, at least half of these are effectively mirror-symmetric since $\|F_{1,2}| - |F_{2,1}\|$ is less than the standard deviation in the measurements. The 16 transforms were averaged in Table I to maintain $|F_{1,2}| > |F_{2,1}|$, but the reconstructed image produced from this average is not distinguishable from the average obtained preserving the original direction of view.

The structure factor amplitudes listed in Table I show that, at the resolution of these data, only the [1, 2], [2, 1] pair (that have an average ratio of 2.8) contribute significantly to the asymmetry of the low-irradiation image. The other structure factors with $h \neq k$ that are significantly larger than the variations measured among specimens (for both low and high-irradiation images) are the [1, 3], [3, 1] pair; but the differences for this pair are comparable to the standard error of the mean. Analysis of the deviations in the data summed in Table I provides a measure of statistical reliability of the averaged structure factors. Although 15 structure factors have been calculated to a resolution of 14.5 Å, only nine of these out to a resolution of ~20 Å are definitely statistically significant in

the average of the low-irradiation images. The effective resolution of the high-irradiation images, from the statistics of the transform averages, is somewhat lower; and the departure of these images from mirror symmetry (for plane group p6m) are not significant.

Reconstructed Low-irradiation Images

Reconstructed images from 25 processed low-irradiation, well-ordered junction lattices, together with averages of 21 of these are displayed in Fig. 3. The four images at the bottom (*a, b, c, d*) were not included in the averages. All reconstructed images are displayed as originally viewed; of those included in the averages shown at the top of Fig. 3, the 11 left-handed images are grouped on the left (L1–11) and the 10 right-handed ones on the right (R1–10). $\bar{L}$ is the average of L1–11 and $\bar{R}$ the average of R1–10; A_L and A_R are averages of all 21 converted to the same hand and displayed as left- and right-handed, respectively.

There is obvious variation in the appearance of the individual images (Fig. 3) included in the averages, but the angle by which the hexameric unit is skewed to the left or right of the lattice vectors is very similar for all images. This skewing is measured in reciprocal space by the asymmetry in amplitude of $F_{1,2}$ and $F_{2,1}$. The magnitude of the difference for this pair of structure factors is relatively constant for all our low-irradiation images corresponding to the similarity of the skewing seen in real space.

The similarity of different images can be measured in reciprocal space by the R factor comparing their scaled structure factors. A small R factor between a pair of image transforms corresponds to similar Fourier components and therefore a close correspondence in the pair of images. R-factors for the left-handed images were calculated relative to their average ($\bar{L}$) and similarly for the right-handed ones relative to their average ($\bar{R}$). The images in Fig. 3 are grouped roughly according to their R-factors, as listed in the key, with those closest to their average at the top. Arrangement according to R-factor was not followed exactly in order to juxtapose images comparing particular details. For example, some images are grouped according to increase or decrease in the amount of stain seen at the connexon center compared to the average. Since images can differ in more than one way from the average, the R-factor measuring the difference from the average does not provide a unique criterion for measuring interrelations.

Variability

Variations among images of junctions from the same preparation—even from the same grid or in the same micrograph—are comparable to variations in images from different specimens prepared at different times. For example, L3 and L11 from the same preparation differ significantly, whereas L3 is similar to the average and several images from other preparations. The range of variation within the six specimen preparations we have examined are illustrated in two sets: preparation I (L1, 2, 4, 6, 8; R1, 3, 7, 9, and *c*) and preparation II (L5, 9; R2, 4, 5, 6, 8, and *d*). L1, L4, R1, R3 from preparation I, imaged in the same micrograph, are very similar to each other; in contrast L5, R2, R4, R5 from preparation II, imaged together in another micrograph, show considerable differences in the amount of stain at the connexon center. Images, which differed significantly from the rest (R factor >70%), that were not included in the averages are shown in Fig. 3 *a, b, c,* and *d*. The pair a-L10 is from adjacent junction images recorded in the same micrograph; and the pair b-L11 is from another micrograph. The image in Fig. 3 *c* is from a grid that retained very little negative stain and differed obviously from normally

TABLE I

Comparison of Averaged Structure Factors $\bar{F}_{hk}$ of Gap Junction Images

			$\bar{F}_{hk} \pm (\sigma/\sqrt{n})$*			
$h^2 + hk + k^2$	h	k	New (21 images)	Conventional (16 images)	Type A‡ (3 images)	Type B‡ (3 images)
1	1	0	622 (43)	200 (53)	329	
3	1	1	−240 (52)	−1,000 (34)	−929	−872
4	2	0	−433 (33)	−966 (12)	−561	−670
7	2	1	−233 (29)	−113 (14)	103	−148
	1	2	−655 (34)	−166 (11)	126	−182
9	3	0	138 (14)	−20 (12)	−70	−44
12	2	2	42 (9)	−51 (12)	−144	−143
13	3	1	105 (17)	−26 (7)	−116	−103
	1	3	76 (16)	−23 (8)	−126	−118
16	4	0	−11 (5)	−15 (5)	−75	−99
19	3	2	−12 (6)	−3 (3)		
	2	3	−6 (3)	−1 (2)		
21	4	1	−5 (4)	1 (2)		
	1	4	−11 (7)	−2 (2)		
25	5	0	−2 (3)	2 (2)		
$\lvert F_{1,2}\rvert - \lvert F_{2,1}\rvert \pm [(\sigma^2_{1,2} + \sigma^2_{2,1})/n]^{1/2} =$			422 (45)	53 (18)	23	34

Structure factors, F_{hk}, for the four image reconstruction averages displayed in Fig. 5 are listed in order of their reciprocal lattice spacing ($d^*_{hk} = (2/\sqrt{3}\,a)(h^2 + hk + k^2)^{1/2}$, where the lattice constant $a = 84 \pm 2$ Å for our new and conventional images and $a = 85$ Å for the Type A and B images). Averages have been computed with F_{hk} inverted as necessary to maintain $|F_{1,2}| > |F_{2,1}|$ corresponding to a left-handed lattice. The standard error of the mean, $\sigma/\sqrt{n}$, computed for each of our structure factors from the n values averaged, provides an objective measure of the significant differences between individual data points. Higher resolution structure factors (beyond the [4, 0] term), which are comparable to the deviations in the measurements, are not statistically significant in the averaged transforms.

* $\sigma/\sqrt{n}$ is the standard error of the mean, where σ is the standard deviation of the measurement and n is the number of lattices measured; $n = 21$ for the new low-irradiation average and $n = 16$ for the conventional average.

‡ Data of Zampighi and Unwin (33) from three lattice domains each for the two forms of gap junction they designate A and B. Standard error of the mean is not given for these data since the sample sizes are small.

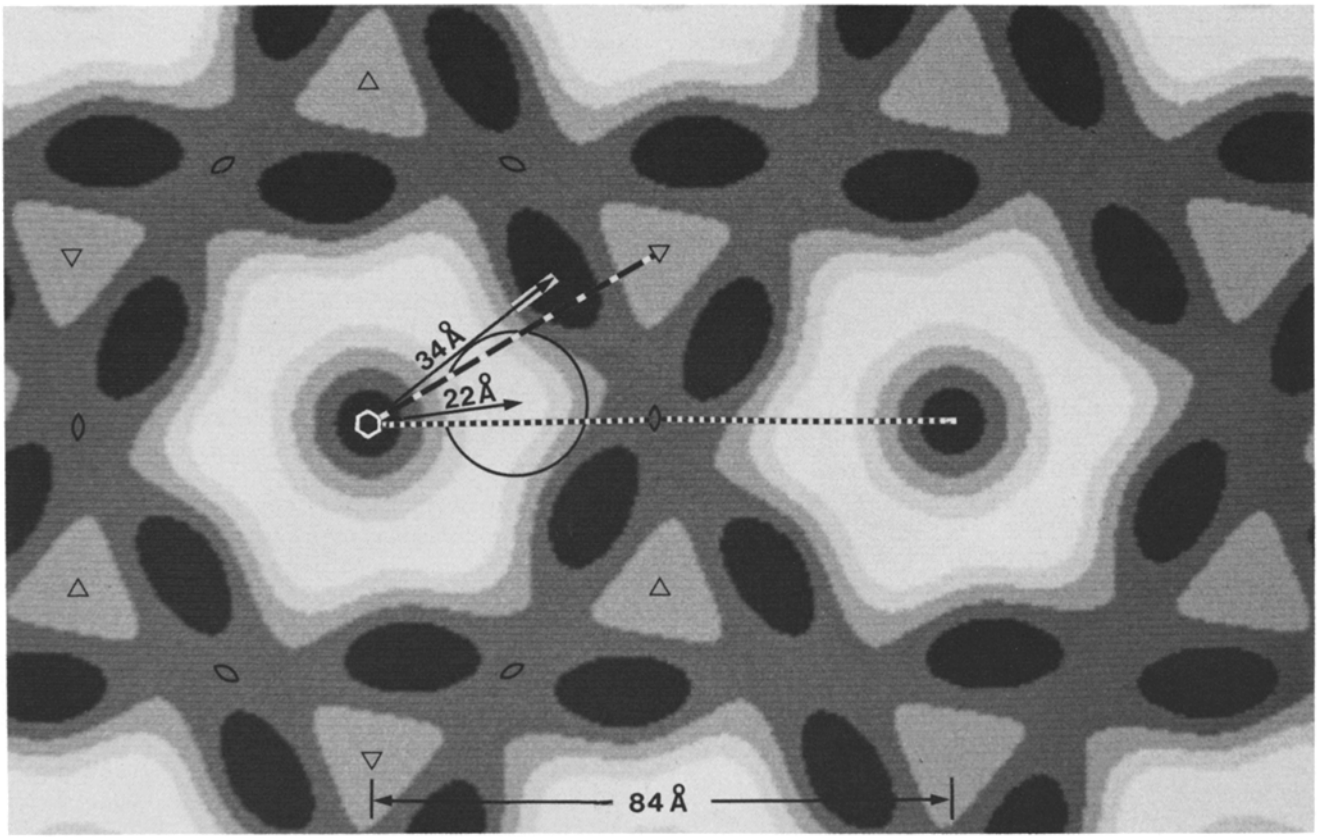

FIGURE 4 Characteristic features of low-irradiation image. Averaged image from 21 low-irradiation gap junction lattice domains (A_L from Fig. 3), contoured on a five-step grey level display, illustrates the dominant features in the negatively stained structure. Stain is concentrated in the lattice on the sixfold axis and at a site about 34 Å from the connexon center at an angle of 8° to the [1, 1] lattice vector (direction from sixfold to threefold axis). The domain of one stain-excluding lobe of the connexon image is indicated by the 11-Å radius circle centered 22 Å from the sixfold axis at an angle of 8° to the [1, 0] lattice vector. There is a relative paucity of stain in the triangular region at the threefold axis.

stained specimens. The specimen in Fig. 3 *d* was treated differently from the rest: it was positively stained with 10^{-4} M uranyl acetate, centrifuged and resuspended in water before applying to the grid. The differences in appearance in Fig. 3 *c* and *d* compared to other specimens are correlated with different staining conditions. The image variations in the normally stained specimens appear to be due more to local differences in staining conditions than to intrinsic differences in the junction preparations.

Characteristic Features

Characteristic features common to all images are evident in Fig. 3 despite the wide range of variation in appearance. The principal features are indicated in Fig. 4 which is a five step grey level display of the average junction image A_L from Fig. 3. The dominant concentrations of stain are on the sixfold axis of the connexon and in six equivalently related regions at ~34 Å from the connexon center. The peripheral concentrations of stain define the six lobes of the connexon image which can be represented by six circles of diameter 22 Å centered at a radius of 22 Å from sixfold axis. The peripheral concentrations of stain also demark the triangular region, deficient in stain, centered on the threefold axis of the lattice.

The skewing of the hexameric connexon image is defined by the angle of 8° between the [1, 1] lattice vector (from sixfold to threefold axes) and the vector from the connexon center to the peripheral concentration of stain. Because the stain concentrations are symmetrically shaped, the stain excluding region, which represents the connexon image, appears nearly mirror-symmetric. A consequence of this local mirror symmetry is that the angle between the [1, 0] lattice vector and the vector from the sixfold axis to the center of the lobe of the connexon image is also 8°. The noncrystallographic mirror lines of the connexon image are all inclined at the 8° angle to adjacent principle lattice vectors. The skewing of the peripheral concentrations of stain relative to the lattice vectors accounts for the large asymmetry in the amplitudes of the [1, 2] and [2, 1] spots in the diffraction pattern.

The variation in the appearance of the individual images in Fig. 3 is largely a consequence of differences in the relative amount of stain at the connexon center and in the space between connexons. The constancy of the size and shape of the connexon image results because the position of the stain concentrations at ~34 Å from the center outlining this image are relatively invariant. Variation in the amount of stain at the connexon center is evident in different images (compare L5, L7 with L9, R8, L11). The large apparent variation in staining on the threefold axis (compare R4, L11 and L6, L8) may involve relatively small differences in stain distribution since the contrast in this region is small compared to that in the connexon image (cf., Fig. 4).

The self-consistency of the image feature illustrated in Fig. 4 is demonstrated by the close correspondence of the independent averages $\bar{L}$ and $\bar{R}$ of left- and right-handed images in Fig. 3 when inverted to have the same hand. The R-factor

comparing the transforms of these two averages is 42% if compared directly, but if the transform of either is inverted, the R factor is reduced to 13% which is less than that between any pair of individual images. Thus, from the information available in the images, the structure of the negatively stained junctions producing left- and right-handed images cannot be distinguished when compared with the same hand.

DISCUSSION

Comparisons of Images

Our low-irradiation images of uranyl acetate stained gap junctions consistently show an asymmetrically oriented, hexameric connexon image with less stain at the threefold axes of the lattice than at the periphery of the connexon (Fig. 3). The fact that these features have not been observed before under conventional imaging conditions may be a consequence of the acute sensitivity of the stain distribution to electron irradiation (Fig. 1). Low-irradiation images obtained by Henderson et al. (14) from mouse liver gap junctions, isolated with a nonionic detergent and negatively stained with phosphotungstate, do show hexameric connexons skewed in the lattice with about the same twist as we have measured. They report, however, that similar images were also obtained with normal electron doses. The diffraction pattern from a low-irradiation image in their paper shows asymmetry in the intensity of the [1,2], and [2,1] spots, but the stronger one of the pair is weak compared to the lower order spots. Because that diffraction pattern is dominated by the low-resolution spots, their optically filtered image does not show much resolved substructural detail. The stain distribution between the connexons in their images appears uniformly dense, unlike our images which show less stain on the threefold lattice axis.

In contrast to the skewed arrangement of connexons seen by Henderson et al. (14) and by us, reconstructed images calculated by Zampighi and Unwin (33) from low-irradiation micrographs of two forms of rat liver gap junctions, negatively stained with uranyl acetate, show hexagonal shaped connexons in projection, which appear to be arranged with mirror symmetry in the lattice. The highest concentration of stain between connexons in their images is on the threefold axis. Mirror-symmetry in their processed images (33) resulted because they "rejected the micrographs that gave patterns in which the [1,2] peak was strongly enhanced relative to the [2,1] (or vice versa)." This choice was based on the assumption "that the two halves of the gap junction are equivalent, but face in opposite directions ... and therefore that the more symmetrical optical diffraction patterns ... implied more even staining throughout their thickness." Furthermore, they reported that "generally, the more symmetrical the diffraction, the higher the resolution to which it extended." Fourier transforms calculated by Unwin and Zampighi (32) from similarly selected micrographs of gap junction lattices, tilted to provide three-dimensional data, showed only minor departures from the symmetry of the two-sided hexagonal plane group p622. They concluded that the two halves were almost equivalent and that the departures from perfect symmetry were probably produced by differences in staining at the top and bottom surface.

In selecting gap junction micrographs for image processing, we did not impose the condition that the optical diffraction pattern show mirror symmetry (e.g., [1,2] and [2,1] spots of comparable intensity). Our criteria for selection were that the optical diffraction patterns should show sharp spots out to at least the third order with no obvious indication of specimen distortion or imperfect electron-microscope imaging conditions. Contrary to the expectation that uniformly stained specimens should show mirror symmetry, the 24 negatively stained junction lattice domains from low-irradiation micrographs that we first selected for image processing all showed pronounced asymmetry in the intensity of the [1,2], [2,1] pair of diffraction spots. We then searched through our micrographs to try to find well-ordered lattices with mirror-symmetric diffraction patterns: only one such example was found, but examination of the micrograph revealed that it consisted of two gap junction lattices in almost perfect face-to-face register from a flattened, vesiculated junction. We cannot explain why we did not observe some junction lattices with approximate mirror-symmetry in our low-irradiation micrographs, since our procedures for microscopy are similar to those used by Zampighi and Unwin (33), who did find such images. However, we have not compared specimens prepared using their protocol which limits endogenous proteolytic activity. Our failure to find mirror-symmetric, low-irradiation images cannot be attributed to any asymmetry in the microscope or image processing, since identically processed high-irradiation micrographs consistently gave nearly mirror-symmetric diffraction patterns (Fig. 1 *c* and *k*).

Table I compares our averaged structure factors for low-irradiation and conventional, high-irradiation gap junction images with those calculated by Zampighi and Unwin (33) from their A and B type specimens. The reconstructed images from these four averaged transforms are shown in Fig. 5. Table I and Fig. 5 summarize the available computer processed image data from untilted gap junction specimens. Our low-irradiation averaged image (Fig. 5 *c* and *d*) shows relatively little stain on the connexon axis whereas the B-type specimen (Fig. 5 *g* and *h*) shows the most. A striking characteristic of our low-irradiation images is paucity of stain on the threefold axis and the nearby concentration of stain between the lobes of the hexameric connexon unit that is skewed relative to the lattice axes. This appearance contrasts with the other three images in Fig. 5 which show a more uniform distribution of stain between connexons with a maximum on the threefold axis. The data in Table I have been scaled to equate the sums of the structure factors (see Materials and Methods) which makes the overall density fluctuations in the images in Fig. 5 similar to each other. The contrast in our low-irradiation micrographs is, however, significantly less than that of the three other types of specimens; thus, the absolute differences in the amount of stain among these specimens may be even greater than indicated in Fig. 5.

Skewing of Connexons in Lattice

Skewing of the connexon images in micrographs of the gap junction lattice may display an intrinsic asymmetry of the membrane pair or it may result from asymmetric staining or distortion of an intrinsically symmetric pair of membranes on the support film. If the two membrane lattices that form the junction were equivalently related, then there would have to be twofold axes in the plane of the gap oriented parallel to the principal lattice axes; and these twofold axes would appear as mirror lines in an undistorted projected view normal to the surface. If the stain were concentrated on one surface, the image need not have mirror symmetry. Such a surface would appear to have the opposite hand when viewed from opposite sides. Thus, if some junctions were stained on the side near the support film and others on the side away, they could appear to

have opposite hand. However, when such asymmetric staining has been observed in other structures that should have mirror symmetry in projection, the near side and far side views are often not exactly the inverse of each other since surface forces on drying tend to deform the two sides differently (9, 23). Furthermore, switching from dominant near side to far side staining can occur from one part to another of such a periodic assembly and nearly mirror-symmetric images may be observed where the staining is about equal on the two sides (23, 24). In contrast to asymmetric staining, uniform staining of gap junctions in which the local symmetry axes of connexon pairs are skewed relative to the lattice axes would show arrays with opposite hand depending on which side of the asymmetric membrane pair were in contact with the support film.

All our observations on low-irradiation gap junction micrographs are consistent with the supposition of an intrinsically asymmetric membrane pair structure. Left- and right-handed images occur with just about equal frequency as expected for random settling of one side or the other in contact with the support film. Junctions lying next to each other on the grid are found with opposite hand (e.g., Fig. 3, L5 and R4); but change of hand has not been observed within the same junction lattice domain, nor have any regions been seen which have mirror symmetry. (The projected image of a symmetric membrane pair lattice would appear mirror-symmetric if it were equally stained on both sides; change in hand of the lattice image could occur if the staining switched from dominant on the near side to dominant on the far side in different parts of the same lattice domain.)

Reconstructions of the overlapped images of two parts of a junction lattice that had folded back on itself are of opposite hand (Fig. 3, L4 and R1) as expected for views from opposite sides of a uniformly stained, skewed array of connexon pairs. Also, a flattened junction vesicle (not shown), with the overlapped top and bottom membrane-pair lattices in nearly perfect register, gave a mirror-symmetric diffraction pattern as expected for exact superposition of two lattices of opposite hand. Asymmetric staining could provide an alternative explanation of the opposite hand for views from opposite sides of the folded-over junctions if the dominant contrast resulted from stain concentrated either at the interface or on the outside surfaces. However, edge on views of our junction specimens (cf. upper right of Fig. 1 *e* and *i*) show that the gap is strongly contrasted, and it is very unlikely that the stain is asymmetrically distributed across the ~30-Å wide gap.

The positively stained image of six concentrations of stain at the connexon periphery (Fig. 3 *d*) shows the same skewing observed in negatively stained images which is unlikely to be the result of asymmetric staining (although specimen distortion on drying could introduce asymmetry). The very close similarity of the independent averages of the left and right handed reconstructions (Fig 3. $\bar{L}$ and $\bar{R}$) when compared with the same hand (R-factor 13%) suggests that these are views in the opposite direction of the same structure.

Compelling as our evidence is for intrinsic asymmetry of the two halves of the junction lattice, it does contradict the *a priori* expectation that identical connexons hexagonally arrayed in the two connected membranes should behave equivalently (6). *Ad hoc* arguments could be constructed to support the expectation of symmetry, but there are, in fact, no physical requirements that identical units all pack in the same way in a periodic assembly. Noncrystallographic symmetry is commonplace in laboratory grown crystals of protein structures; and among stable biological assemblies, the polyoma virus capsid, in which pentameric morphological units are six-coordinated (27), provides a striking example of nonconservation of bonding specificity. Because the projected image of the connexon pair appears mirror symmetric, each pair may be a symmetric dimer of identical connexon hexamers. The twofold axes of such dimers in a skewed lattice arrangement would be noncrystallographic symmetry axes: this implies that the side-to-side hexagonal bonding interactions of the connexons would have to be different in the two paired membrane lattices.

The structural basis of the asymmetry observed in the face-on view of gap junction lattices will be clarified by three-dimensional reconstruction of this structure from tilted views of minimally irradiated specimens. To obtain reliable images of the same structure viewed in different directions, the radiation sensitivity needs to be quantitatively assessed and conditions for obtaining reproducible staining needs to be established.

Variable and Conserved Image Features

We presume that all the gap junctions we have examined start out with the same structure. This presumption is born out by x-ray diffraction patterns from similarly prepared specimens which show that the average structure of a large population is reproducible and well-defined. Differences seen in micrographs of individual junctions can result from statistical fluctuations in stain distribution and from local variation in specimen conditions on the grid. What is observed in each reconstructed image (Fig. 3) is the distribution of stain within the repeating unit of the hexagonal lattice (one-sixth of each unit cell) that has been averaged with the lattice periodicity over ~5,400 subunits. Image artifacts due to distortions in the lattices of well-ordered domains are negligably small as indicated by the sharpness of the spots in the diffraction patterns (Fig. 1) and by the regularity of the lattice dimensions (Fig. 2). The variations evident in Fig. 3 can be described in terms of differences in the relative amount of stain in three distinctive parts of the image: (*a*) on the connexon axis, (*b*) in the indentation between lobes of the hexameric connexon, and (*c*) in the space between connexons.

STAIN IN CHANNEL: Differences in accessibility of the connexon channel can account for the darkly stained centers of some images (Fig. 3, L5 and L7) and the virtual absence of stain at the center of others (Fig. 3, L9 and L11). Even among adjacent junction lattices imaged in the same micrograph (Fig. 3, L5, R2, R4, and R5), differences in stain accumulation at the connexon center do occur that may reflect local alterations in the structure. The apparent size of the axial channel increases from ~10 to ~25 Å with increasing density of stain; this correlation indicates that the actual dimension of the stained channel is less than or comparable to the resolution limit (~20 Å) of the reconstructed image.

STAIN AT CONNEXON PERIPHERY: The lobes of the hexameric connexon evident in all the reconstructed, negatively stained images (Fig. 3) are a consequence of the six concentrations of stain at the connexon periphery. This stain concentration is located in the averaged image at a radius of 34 Å from the connexon center, 8° away from the [1,1] lattice vector (Fig. 4). There is very little variation in the location of this feature in the individual negatively stained images (Fig. 3). The range of variation in density of this stain at the connexon periphery is less than that at the center.

Weakly negatively stained (Fig. 3 *c*) and positively stained (Fig. 3 *d*) specimens give the initial impression of reversed

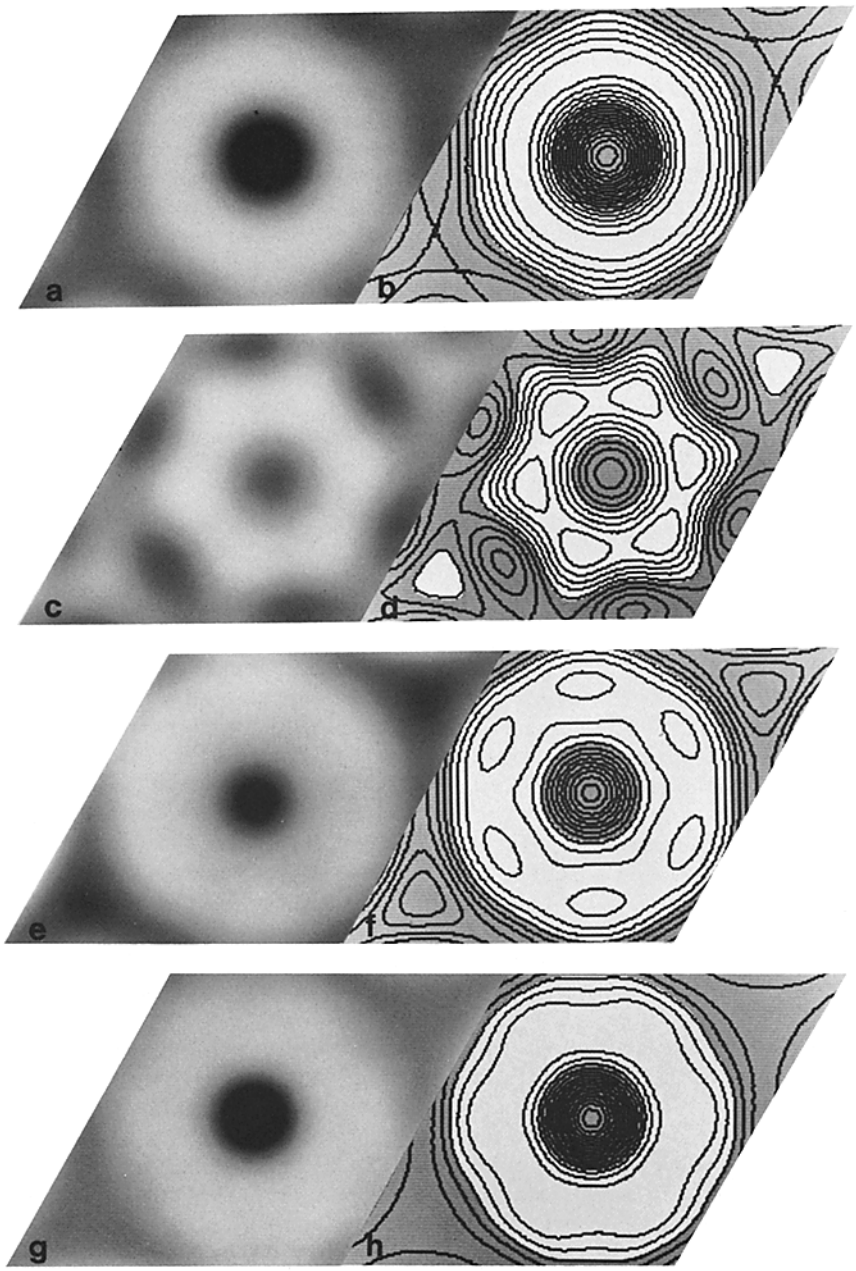

FIGURE 5 Comparison of the new image with other computed reconstructions. Reconstruction averages of: (*a* and *b*) 16 conventional, high-dose images (including Fig. 1 *d*); (*c* and *d*) 21 low-irradiation images (identical to A_L of Fig. 3); (*e* and *f*) three low-irradiation Type A images (33); and (*g* and *h*) three low-irradiation Type B images (33). Each reconstruction of the contents of a single unit cell is plotted as a 256 grey level display on the left and as a contour map (with regions of negative density shaded) on the right. Fourier transforms of the four images were scaled as described in the Materials and Methods section. The zero level contour corresponds to the average density which has been fixed by setting $F_{oo} = 0$.

contrast at the connexon periphery. Measurements show, however, that the hexameric stain concentration in these images is at a radius of ~30 Å, twisted 8° to the [1,1] lattice vector. Thus, the same feature at the connexon periphery appears to be revealed by negative and positive staining. Consistent staining of such a site with high affinity for uranyl acetate could account for the relatively invariant dimensions and orientation of the hexameric stain-excluding region in different junction images.

STAIN BETWEEN CONNEXONS: The amount of stain between connexons appears quite variable. The positively-stained (Fig. 3 *d*) and weakly negatively stained (Fig. 3 *c*) specimens are at one extreme with no stain visible beyond the connexon periphery. Fig. 3 *a* shows a specimen with slightly more stain, which gives the appearance of a large clear triangular region at its threefold axis; another junction is this micrograph (Fig. 3, L10) has more stain beyond the connexon periphery leading to a smaller unstained triangle. Other specimens (Fig. 3, R4 and L11) show fairly uniform staining between the connexons with only slightly less stain at the threefold axis than at the connexon periphery. The large apparent variability in the stain distribution about the threefold axis is related to the relatively low contrast between features in this region. Thus, a small change in the amount of negative stain between connexons can lead to a large difference in the appearance.

Interpretation of Variations in Images

The morphological variation evident among the images in Fig. 3 can be interpreted in terms of (*a*) significant differences in stain penetration of the axial channel, (*b*) relatively invariant stain localization at the connexon periphery, and (*c*) a moderately variable amount of stain in the space between connexons. Some of the image variation is due to statistical fluctuations in stain distribution in junctions with the same structure. The variations seen in Fig. 3, L1, L2, L3, R1, R2, and R3, may be accounted for by such fluctuations. The R-factors comparing the Fourier transforms of these images with the averaged values are in the range 16–22% which is comparable to the deviations from perfect hexagonal symmetry in the p1 averaged images. This range of variation can reasonably be attributed to statistical fluctuations. Alternatively, variation in the amount of stain at the connexon center may reflect intrinsic alterations in the specimen due to local environmental stresses. Local staining conditions could also account for differences in the amount of stain between connexons. The images could be sorted into subcategories (e.g., dark vs. light centers) that may correspond to distinguishable staining states of the specimens.

Differences in the junction images (Fig. 3) do not, by themselves, constitute reliable criteria for distinguishing different junctional states since our negatively stained specimens were all prepared following, as closely as possible, the same procedures. Zampighi and Unwin (33) have distinguished a B state (Fig. 5 *g* and *h*) in their specimens exposed to deionized water for several days which show some differences in appearance compared to their A state specimens (Fig. 5 *e* and *f*) that had not received this water treatment. Unwin and Zampighi (32) have interpreted three-dimensional reconstructions of their two types of specimens in terms of a model that switches from open in the A state to closed in the B state. Their maps, however, appear to show more stain in the axial channel between the pair of connexons in the "closed" B form than in the "open" A form.

Gap junctions, when isolated from the intact tissue, should be in the high resistance state since cellular damage leads to uncoupling of junctional communication (18). This is consistent with x-ray diffraction data from isolated junctions in sucrose solutions which indicate that the channel along the axis of the connexon pair, extending across the gap, is inaccessible to sucrose, being somehow closed at both cytoplasmic surfaces (21). Electron micrographs showing a weakly stained connexon center (Fig. 3, L9, 11, and R8; and reference 14) may represent a better preserved state of the isolated junction structure than the more familiar image with a darkly stained center. The extent to which stain may penetrate the channel appears to be influenced by specimen preparation procedures, by the staining conditions, and by effects of irradiation.

Radiation Sensitivity

Our negatively stained gap junction specimens are acutely sensitive to electron irradiation (Fig. 1). The low-irradiation image is converted to the conventional appearance following an electron dose less than that normally used in microscopy. Displacement of stain from the connexon periphery may account for the conversion of the skewed, six-lobed connexon (Fig. 5 *c* and *d*) into a doughnut shape with smooth hexagonal outline, oriented with mirror symmetry in the lattice (Fig. 5 *a* and *b*). Irradiation appears to increase the size of the connexon but the diameter measured at the zero level contour is the same as the maximum diameter of the low-irradiation image. Radiation-induced stain movement (3, 30), rather than change in connexon dimensions and orientation, can account for this gross alteration in morphological appearance. Disappearance of the triangular low density feature (Fig. 5 *c* and *d*) may result from redistribution of stain between connexons (Fig. 5 *a* and *b*) to fill a vacancy on the threefold axis. Alternatively, stain may be excluded by matter on the threefold axis that is modified by irradiation or obscured by stain movement at another level. Irradiation significantly increases the amount of stain at the connexon center which implies substantial stain movement in the incinerated specimen. If consecutive images can be recorded at very low-irradiation levels, it may be possible to follow the kinetics of the radiation-induced stain redistribution. Three-dimensional reconstruction will be required to map the location of the stain concentrations in the structure. This information will be essential for visualizing the intrinsic structure of gap junction membranes.

Comparison of Isolation Procedures

Isolation procedures influence the extent of proteolytic cleavage of the junction protein, curvature of the paired membranes and regularity of the hexagonal lattice. It is possible that the skewing of the connexons in the lattice may also be affected by different isolation procedures. Because there is no functional activity that can be assayed for in isolated junctions, the criteria for a satisfactory purification have been chemical homogeneity and morphological regularity.

All published procedures for purifying mouse and rat liver gap junctions involve initial isolation of a plasma membrane fraction in low ionic strength carbonate buffer (1–10 mM $NaHCO_3$, pH 7.4–8.0). In the procedure we have used (8) the initial extraction medium also contains 1 mM EGTA, which leads to larger yields of junctions than the previous protocol with only 1 mM $NaHCO_3$ (11). Other protocols add calcium (0.5 mM $CaCl_2$, 2 mM $NaHCO_3$, pH 7.4 [25]), or add magnesium with removal of calcium (1 mM $MgCl_2$, 0.5 mM EGTA, 10 mM $NaHCO_3$, pH 8 [33]); in both these procedures, phenylmethylsulfonyl fluoride was added to reduce endogenous proteolysis.

Different detergent treatments have been used to solubilize nonjunctional membranes: in the Fallon and Goodenough (8) protocol, 0.5% sarkosyl NL97 is followed by 0.1% Brij 58; Nicholson et al. (25) used 0.09% sarkosyl together with 1 M urea; Henderson et al. (14) used 5% Triton X-100 with 6 M urea in 2 mM EDTA; and Zampighi and Unwin (33) used 2% sodium deoxycholate followed by 0.1% Lubrol WX. Brij and Lubrol, which are both polyoxyethyleneglycol cetylalcohol detergents, enhance the crystallinity of the connexon arrays in the purified junctions. Some effects of different detergent treatments on the lattice constant have been noted (21), but no specific effects on connexon morphology have been reported.

The molecular weight of the unproteolyzed connexin protein from rat liver appears to be ~28,000 (25) and ~26,000 from mouse liver (14); in both these preparations the yield is only about a quarter of that with the EGTA protocol (8) in which endogenous proteolysis reduces the molecular weight of most of the connexin subunits to about 21,000. The morphology of junction lattices isolated with and without endogenous proteolysis are similar. Furthermore, trypsin treatment, which removes some protein from the cytoplasmic surfaces, does not appear to alter the structure of the connexons in the interior of the bilayer or in the gap (21).

Junctions isolated by the Fallon and Goodenough (8) pro-

tocol with EGTA are often vesiculated; trypsin treatment induces vesiculation in the relatively flat junctions isolated by the earlier Goodenough (11) protocol. Published micrographs of sectioned pellets of purified junctions often show curved profiles, but it is unclear what factors in the preparative procedures are significant in determining the curvature of the paired membrane lattices.

Curvature and Skewing

Studies on differentiating granulosa cells (22) and on physiologically stressed ciliary epithelium (26) show that one of the biological responses of some gap junctions is to curve and vesiculate. This vesiculation may be related to uncoupling of intercellular communication. Curvature requires that the connexons be packed differently in the two coupled membranes. Measurement of the curvature indicates that the distance between connexons in the convex and concave cytoplasmic surfaces may differ by ~10% (6). This ability to curve appears to be an intrinsic property of the ordered packing of the connexons, which implies some sort of switching in the regular bonding interactions in the two membrane surfaces.

Skewing of the pairs of connexons in the coupled membranes also implies some specific differences in the lattice interactions on the two sides. There may be no direct relation between curving and skewing of the junction lattice, but the switching in the bonding interactions among connexons could involve similar structural changes in both cases. The junctions isolated by Henderson et al. (14) with only limited endogenous proteolysis appear flat and have skewed connexon lattices, whereas the junctions isolated by Zampighi and Unwin (33) with no detectable proteolysis appear to have predominantly mirror symmetric lattices. Further comparative studies using different isolation procedures are necessary to explore if there are any correlations between the extent of proteolysis, the curvature of the junctions and the skewing of the connexon in the lattice.

The new features that we have consistently observed by low-irradiation microscopy may be intrinsic to the structure of the gap junction. Three-dimensional image reconstruction will be essential to interpret the skewing of the connexon images in the hexagonal lattice, to locate the peripheral stain concentration and the stain-deficient trigonal feature, and to explain the redistribution of stain induced by electron irradiation. Our observation of lattice asymmetry is compatible with the presumption that the pair of hexameric connexon units join in some way to form a symmetric transmembrane channel. Symmetric connexon dimers could assemble with skewed orientation in a regular hexagonal junction lattice if different side-to-side packing of the hexamers in the two coupled membranes were stable. Such asymmetry may have physiological implications regarding the function of the gap junction as a mediator of intercellular communication.

We thank H. Ulloa, D. DeRosier, L. Amos, and R. Henderson for programs.

This work was initiated with National Science Foundation grants PCM77-16271 to DLDC; and PCM77-13955 to DAG. Support from Public Health Service grants CA-15468 from the National Cancer Institute to D. L. D. Caspar and GM18974 from the National Institute of General Medical Sciences to D. A. Goodenough that were awarded for related studies have been utilized to carry on this investigation.

Received for publication 1 June 1982, and in revised form 27 August 1982.

REFERENCES

1. Agar, A. W., F. C. Frank, and A. Keller. 1959. Crystallinity effects in the electron microscopy of polyethylene. *Phil. Mag.* 4:32–55.
2. Baker, T. S., and L. A. Amos. 1978. Structure of the tubulin dimer in zinc-induced sheets. *J. Mol. Biol.* 123:89–106.
3. Baker, T. S. 1978. Preirradiation and minimum beam microscopy of periodic biological specimens. *Proceedings of the Ninth International Congress on Electron Microscopy.* 2:2–3.
4. Baker, T. S. 1981. Image processing of biological specimens: a bibliography. *Electron Microscopy in Biology.* 1:189–290.
5. Bennett, M. V. L., and D. A. Goodenough. 1978. Gap junctions, electrotonic coupling, and intercellular communication. *Neurosci. Res. Program Bull.* 16:373–486.
6. Caspar, D. L. D., D. A. Goodenough, L. Makowski, and W. C. Phillips. 1977. Gap junction structures. I. Correlated electron microscopy and x-ray diffraction *J. Cell Biol.* 74:605–628.
7. Dubochet, J. 1973. High-resolution dark-field electron microscopy. *J. Electron Microsc.* 98:334–344.
8. Fallon, R. F., and D. A. Goodenough. 1981. Five-hour half-life of mouse liver gap-junction protein. *J. Cell Biol.* 90:521–526.
9. Finch, J. T., and A. Klug. 1965. The structure of viruses of the papilloma polyoma type. III. Structure of rabbit papilloma virus. *J. Mol. Biol.* 13:1–12.
10. Friend, D. S., and N. B. Gilula. 1972. Variations in tight and gap junctions in mammalian tissues. *J. Cell Biol.* 53:758–776.
11. Goodenough, D. A. 1974. Bulk isolation of mouse hepatocyte gap junctions. Characterization of the principle protein, connexin. *J. Cell Biol.* 61:557–563.
12. Goodenough, D. A. 1975. Methods for the isolation and structural characterization of hepatocyte gap junctions. *Methods Membr. Biol.* III: 51–80.
13. Goodenough, D. A., and J. P. Revel. 1970. A fine structural analysis of intercellular junctions in the mouse liver. *J. Cell Biol.* 45:272–290.
14. Henderson, D., H. Eibl, and K. Weber. 1979. Structure and biochemistry of mouse hepatic gap junctions. *J. Mol. Biol.* 132:193–218.
15. Henry, A., and K. Lonsdale. 1952. International Tables for X-ray Crystallography.: Symmetry Groups. Vol. I.
16. Holser, W. T. 1958. Point groups and plane groups in a two-sided plane and their subgroups. *Z. Kristallogr.* 110:266–281.
17. Johansen, B. V. 1976. A low-dose pre-irradiation procedure reducing beam damage. *Micron.* 7:145–156.
18. Loewenstein, W. R. 1966. Permeability of membrane junctions. *Ann. N. Y. Acad. Sci.* 137:441–472.
19. Loewenstein, W. R., Y. Kanno, and S. J. Socolar. 1978. Quantum jumps of conductance during formation of membrane channels at cell-cell junction. *Nature (Lond.).* 274:133–136.
20. Makowski, L., D. L. D. Caspar, W. C. Phillips, and D. A. Goodenough. 1977. Gap junction structures. II. Analysis of the x-ray diffraction data. *J. Cell Biol.* 74:629–645.
21. Makowski, L., D. L. D. Caspar, D. A. Goodenough, and W. C. Phillips. 1982. Gap junction structures. III. The effect of variations in the isolation procedures. *Biophys. J.* 37:189–191.
22. Merk, F. B., C. R. Botticelli, and J. T. Albright. 1972. An intercellular response to estrogen by granulosa cells in the rat ovary; an electron microscope study. *Endocrinology.* 90:992–1007.
23. Moody, M. F. 1967a. Structure of the sheath of bacteriophage T4. I. Structure of the contracted sheath and polysheath. *J. Mol. Biol.* 25:167–200.
24. Moody, M. F. 1967b. Structure of the sheath of bacteriophage T4. II. Rearrangement of the sheath subunits during contraction. *J. Mol. Biol.* 25:201–208.
25. Nicholson, B. J., M. W. Hunkapiller, L. B. Grim, L. E. Hood, and J.-P. Revel. 1981. Rat liver gap junction protein: properties and partial sequence. *Proc. Natl. Acad. Sci. U. S. A.* 78:7594–7598.
26. Raviola, G., and E. Raviola. 1978. Intercellular junctions in the ciliary epithelium. *Invest. Ophthalmol.* 17:958–981.
27. Rayment, I., T. S. Baker, D. L. D. Caspar, and W. T. Murakami. 1982. Polyoma virus capsid structure at 22.5 Å resolution. *Nature (Lond.).* 295:110–115.
28. Revel, J. P., and M. J. Karnovsky. 1967. Hexagonal array of subunits in intercellular junctions of the mouse heart and liver. *J Cell Biol.* 33:C7–C12.
29. Salmon, E. D., and D. DeRosier. 1981. A surveying optical diffractometer. *J. Microsc.* 123:239–247.
30. Unwin, P. N. T. 1974. Electron microscopy of the stacked disk aggregate of tobacco mosaic virus protein. II. The influence of electron irradiation on the stain distribution. *J. Mol. Biol.* 87:657–670.
31. Unwin, P. N. T., and R. Henderson. 1975. Molecular structure determination by electorn microscopy of unstained crystalline specimens. *J. Mol. Biol.* 94:425–440.
32. Unwin, P. N. T., and G. Zampighi. 1980. Structure of the junction between communicating cells. *Nature (Lond.).* 283:545–549.
33. Zampighi, G., and P. N. T. Unwin. 1979. Two forms of isolated gap junctions. *J. Mol. Biol.* 135:451–464.